

Intrinsic Electronic Spectra of Cryogenically Prepared Protoporphyrin IX Ions in Vacuo – Deprotonation-Induced Stark Shifts – Electronic Supplementary Information

Wyatt Zagorec-Marks,^{1,2} James E. T. Smith², Madison M. Foreman,^{1,2} Sandeep Sharma², J. Mathias Weber^{1,2,*}

¹JILA, University of Colorado, Boulder, CO 80309, USA.

²Department of Chemistry, University of Colorado, Boulder, CO 80309, USA.

Table of Contents

S1. Correlated Calculations	2
Figure S1.1. A visual comparison of the theoretical and experimental Q _x and Q _y bands.	2
Figure S1.2 The anion natural orbitals (NOs) from the SA-3-CASSCF(4e,4o) calculation.	3
Figure S1.3 The leading configurations in the CI expansion for the anion ground state.....	3
Figure S1.4 The leading configurations in the CI expansion for the anion Q _x (S1) state.....	4
Figure S1.5 The leading configurations in the CI expansion for the anion Q _y (S2) state.....	4
Figure S1.6 The dianion natural orbitals (NOs) from the SA-3-CASSCF(4e,4o) calculation. .	5
Figure S1.7 The leading configurations in the CI expansion for the dianion ground state.	5
Figure S1.8 The leading configurations in the CI expansion for the dianion Q _x (S1) state.....	6
Figure S1.9 The leading configurations in the CI expansion for the dianion Q _y (S2) state.....	6
S2. Model Protoporphyrin (PP-Me) Calculations	7
Figure S2.1. Structure of PP-Me, used to investigate electric field effects	7
Table S2.2 Summary of the point charge locations and their standard deviations	8
Table S2.3 Experimental and simulated effects of charge state.....	9
S3. Frank-Condon Simulation of Free Base Porphyrin	10
S4. Solvatochromic Data	11
S5. Mid-Infrared Spectra of PP	12
S6. Frequencies and Intensities of Vibrational modes of the Q_x Band of Porphine	13
S7. Frequencies and Intensities of Vibrational modes of the Q_x Band of (PP-H)⁻	16
S8. Assignment of FCHT simulation of (PP-H)⁻ under vertical gradient approximation	18

S1. Correlated Calculations

All PySCF input files along with selected analysis scripts are hosted on GitHub at https://github.com/jamesETsmith/ppix_final.

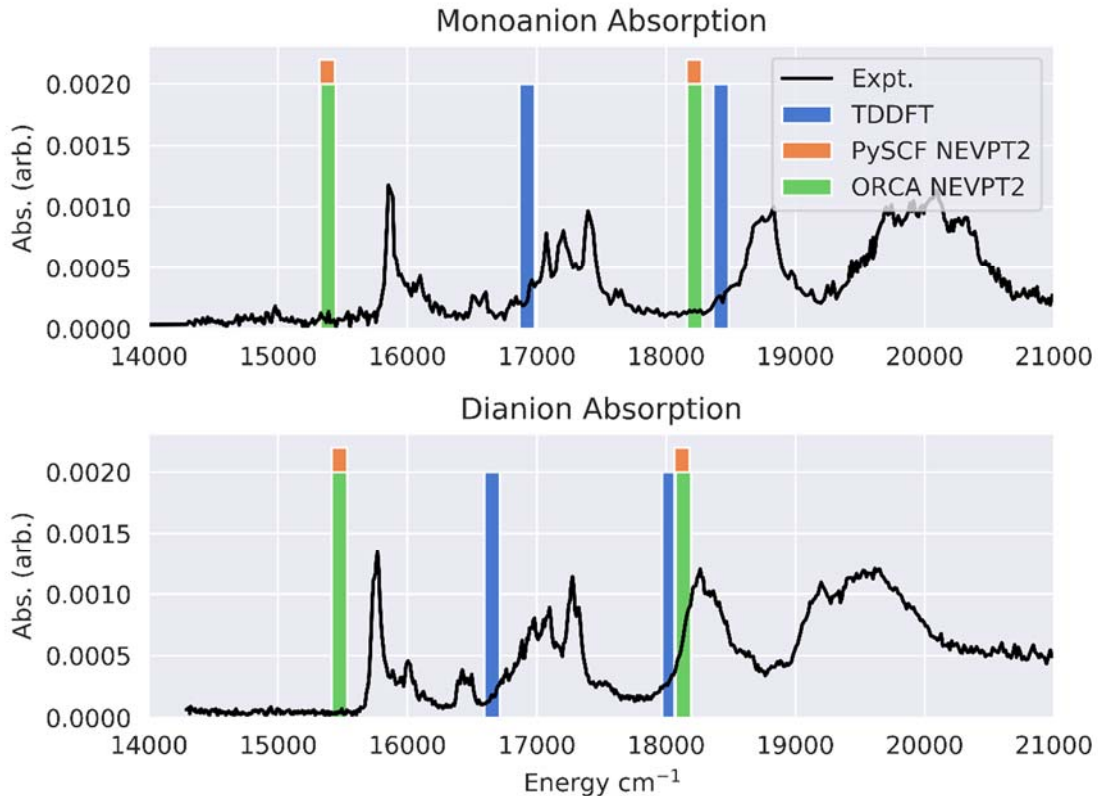


Figure S1.1. A visual comparison of the theoretical and experimental Qx and Qy bands. We make the PySCF NEVPT2 results slightly taller here to facilitate the comparison with the ORCA NEVPT2 results.

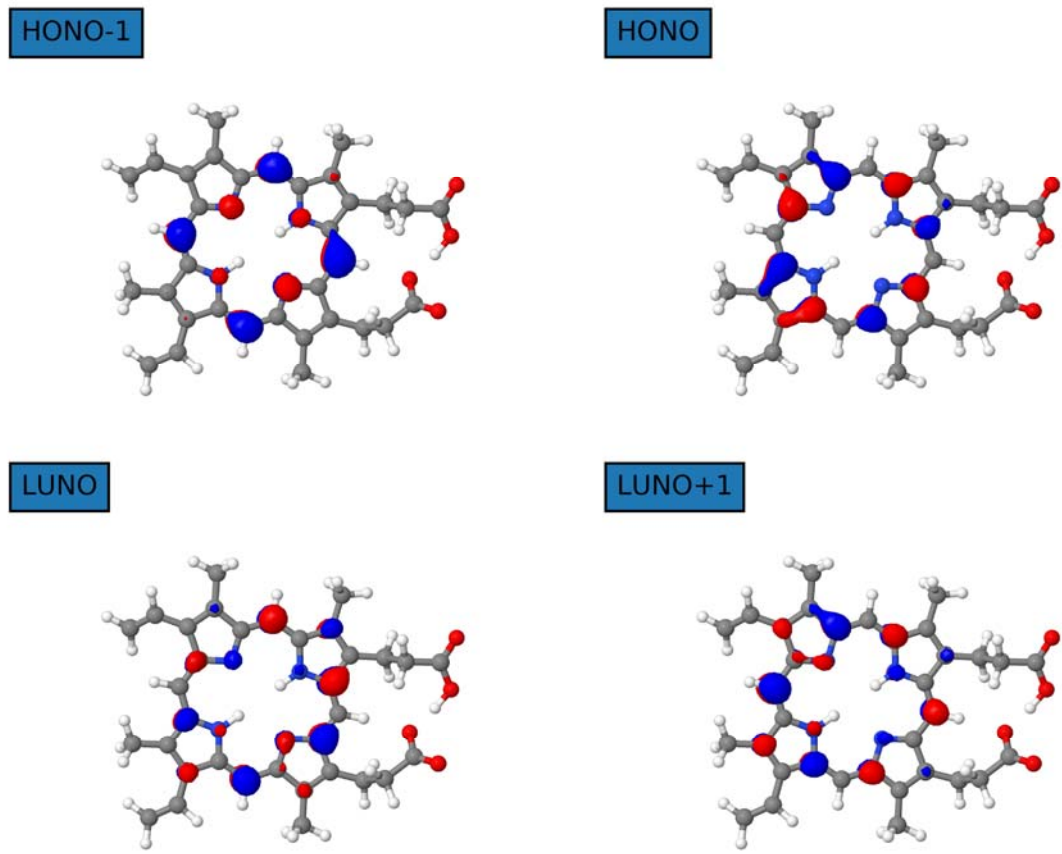


Figure S1.2 The anion natural orbitals (NOs) from the SA-3-CASSCF(4e,4o) calculation.

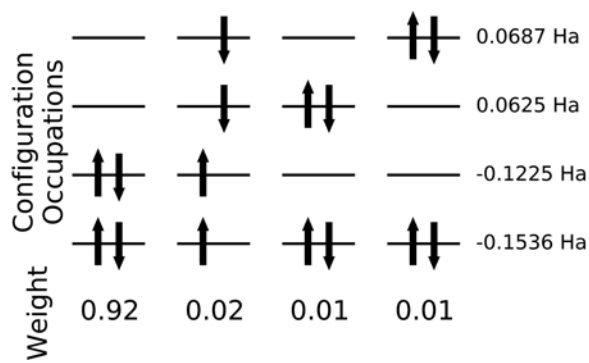


Figure S1.3 The leading configurations in the CI expansion for the anion ground state.

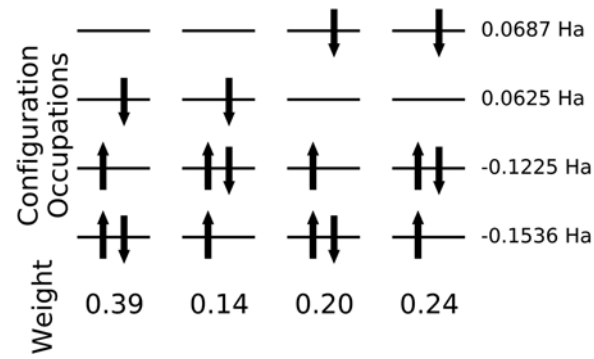


Figure S1.4 The leading configurations in the CI expansion for the anion Q_x (S1) state.

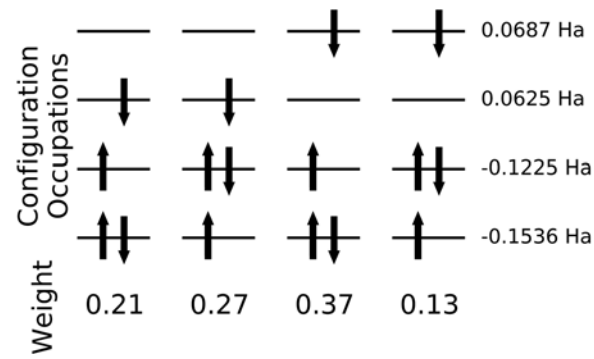


Figure S1.5 The leading configurations in the CI expansion for the anion Q_y (S2) state.

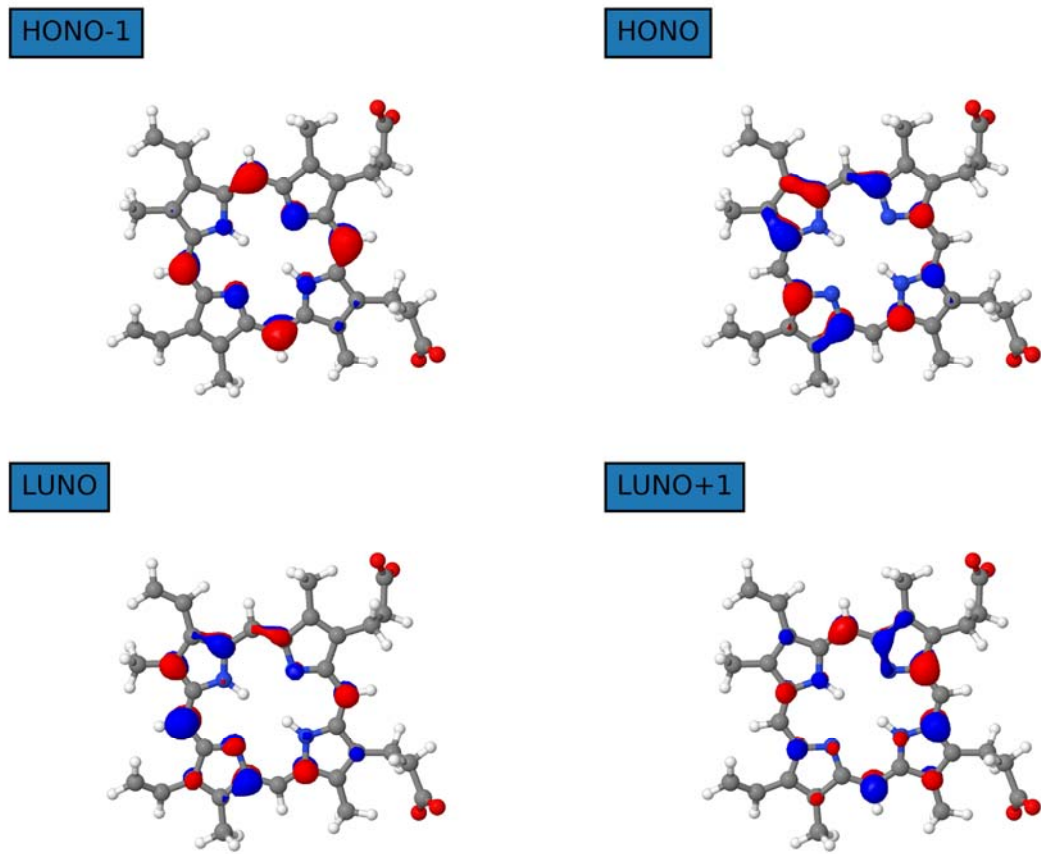


Figure S1.6 The dianion natural orbitals (NOs) from the SA-3-CASSCF(4e,4o) calculation.

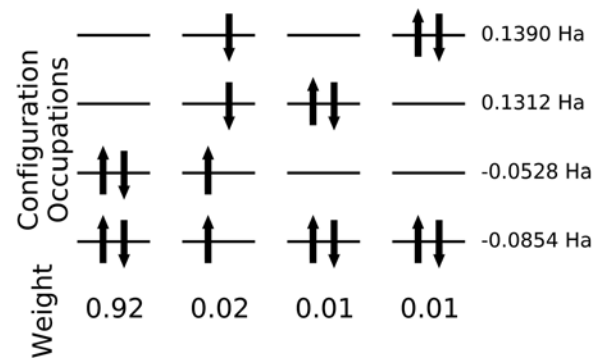


Figure S1.7 The leading configurations in the CI expansion for the dianion ground state.

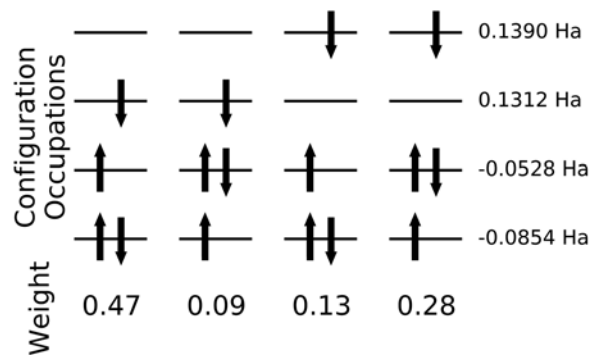


Figure S1.8 The leading configurations in the CI expansion for the dianion Q_x (S1) state.

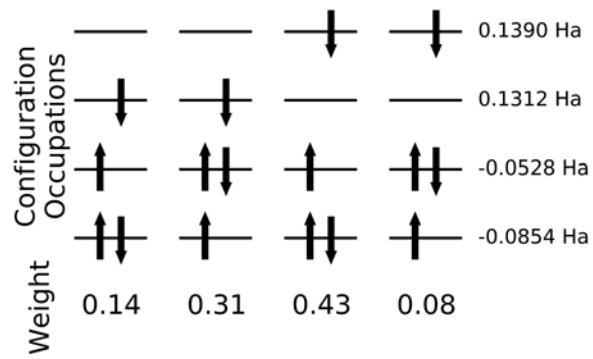


Figure S1.9 The leading configurations in the CI expansion for the dianion Q_y (S2) state.

S2. Model Protoporphyrin (PP-Me) Calculations

Since the NEVPT2 calculations on PP are in good agreement with the experimentally observed splittings, an interesting question in this context is whether NEVPT2 can reproduce the field effects for a simplified model structure that is placed in the field of point charges that approximate the charge distribution of the ions. We calculated the Q_x and Q_y band energies using a modified molecular structure (in the following referred to as PP-Me), where we replaced the charged $(\text{CH}_2)_2\text{COO}(\text{H})$ groups on PP with methyl groups, and placed point charges at different positions to simulate the electric field experienced by the macrocycle in a variety of scenarios. The structure of the macrocycle model was optimized using the ωB97XD functional with 6-31G(d) basis set for all atoms. Figure S2.1 shows the geometry used in these simulations, with three different charge distributions for the monoanion and one for the dianion.

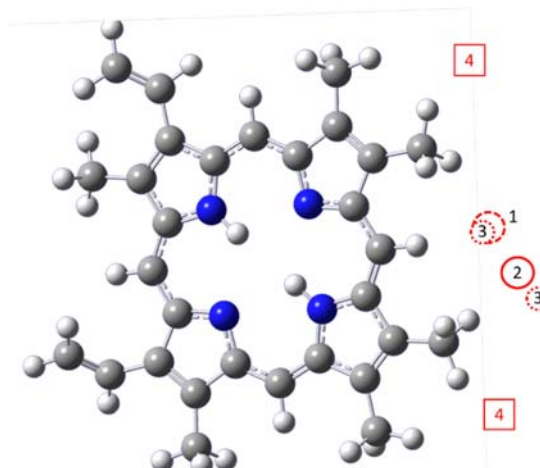


Figure S2.1. Structure of PP-Me, used to investigate electric field effects. Positions marked with numbers represent point charge positions: single point charges ($-e$) were used in positions 1 and 2, two point charges ($-0.5 e$) in each position marked “3”, each configuration simulating a charge distribution modeling the monoanion, and two point charges ($-e$) in each position marked “4” to simulate the dianion structure.

In scenario 1, a point charge of $-e$ is positioned at the location of the deprotonated carboxylate oxygen atom (relative to the macrocycle). In the second scenario, a point charge of $-e$ is placed at the position of the H atom shared between the two carboxylate groups. In the third scenario, two point charges of $-0.5 e$ each are set in the locations of the oxygen atoms involved in the H-bonding between the carboxylate groups. The fourth model charge distribution uses the midpoint between the two oxygen atoms on each carboxylate group as a model for the dianion.

For each scenario, we calculate the position (or positions depending on the scenario) of the point charges using the following procedure:

1. Choose a position for the point charge, e.g. the location of the hydrogen H-bonded between the carboxylate groups in the PP anion.
2. Measure the distance from the point charge to four non-H-atoms, which we refer to as reference atoms, on the porphyrin ring in the PP species.
3. Use the distances and the positions of the same four reference atoms in the PP-Me geometry to calculate the position of the point charge(s) in the new geometry
4. Repeat steps 1-3 for every possible combination of non-H-atoms around the porphyrin ring and take the mean of all coordinates as our point charge location in the correlated calculations.

A summary of the point charge locations and their standard deviations is listed below. All values are in Å.

Table S2.2 Point Charge Coordinates for Model Calculations

Scenario	Charge	X	Y	Z
1	-1.0	-5.7124 ± 0.1298	-3.6452 ± 0.0610	0.1326 ± 0.5764
2	-1.0	-7.0947 ± 0.1190	-3.0432 ± 0.0676	0.1083 ± 0.6237
3	-0.5	-5.7124 ± 0.1298	-3.6452 ± 0.0610	0.1326 ± 0.5764
	-0.5	-8.0172 ± 0.1534	-2.5559 ± 0.0935	0.0854 ± 0.7135
4	-1.0	-2.9263 ± 0.2368	-7.4737 ± 0.2686	-0.3309 ± 1.8030
	-1.0	-8.1490 ± 0.2285	1.2438 ± 0.1640	0.4364 ± 1.5091

Table S2.2 shows the results of these model calculations in terms of the predicted Q_x and Q_y energies. Scenarios 1, 2, and 3 result in similar band energies. Their calculated band energies and splittings are loosely consistent with the calculated results on singly deprotonated PP, but they do not recover the changes observed in going from the mono- to the dianion. The spread of excitation energies from our scenarios indicates that the band positions are quite sensitive to the charge distribution, corroborating our expectation that the local electric field plays a major role for the behavior of the Q band positions. The various scenarios agree qualitatively with the experimental pattern, but they all consistently overestimate the Q_x band energies, while underestimating the Q_y energies. Clearly, the treatment using point charges in the vicinity of a simplified model macrocycle is insufficient to correctly account for the Stark shifts. We caution that the geometries of the PP-Me model structure and the deprotonated PP structures differ sufficiently strongly to introduce uncertainties in the positions of the point charges, depending on which atoms in the macrocycle are chosen as reference atoms. This uncertainty introduces possible errors regarding the electric field experienced by the atoms closest to the charges. These errors range from ca. 5% for the monoanion to ca. 15% for the dianion.

Table S2.3 Experimental and simulated effects of charge state. Vertical transition energies in cm^{-1} .

Charge State	Molecule	Method	$E(Q_x)^{(d)}$	$E(Q_y)^{(d)}$	$\Delta E^{(d)}$
0	PP	experiment ^(a)	15900 ± 100	19050 ± 100	3150 ± 141
	PP	NEVPT2	15810	18606	2796
-1	PP	experiment ^(b)	15870 ± 10	18760 ± 30	2890 ± 32
	PP	NEVPT2	15377	18217	2840
	PP-Me	NEVPT2(1) ^(c)	16072	18530	2457
	PP-Me	NEVPT2(2) ^(c)	16155	18656	2501
	PP-Me	NEVPT2(3) ^(c)	16110	18640	2530
-2	PP	experiment ^(b)	15760 ± 10 (-110)	18270 ± 30 (-490)	2510 ± 32 (-380)
	PP	NEVPT2	15472 (+95)	18123 (-94)	2651 (-189)
	PP-Me	NEVPT2(4) ^(c)	16152 (+40)	18702 (+93)	2550 (-54)

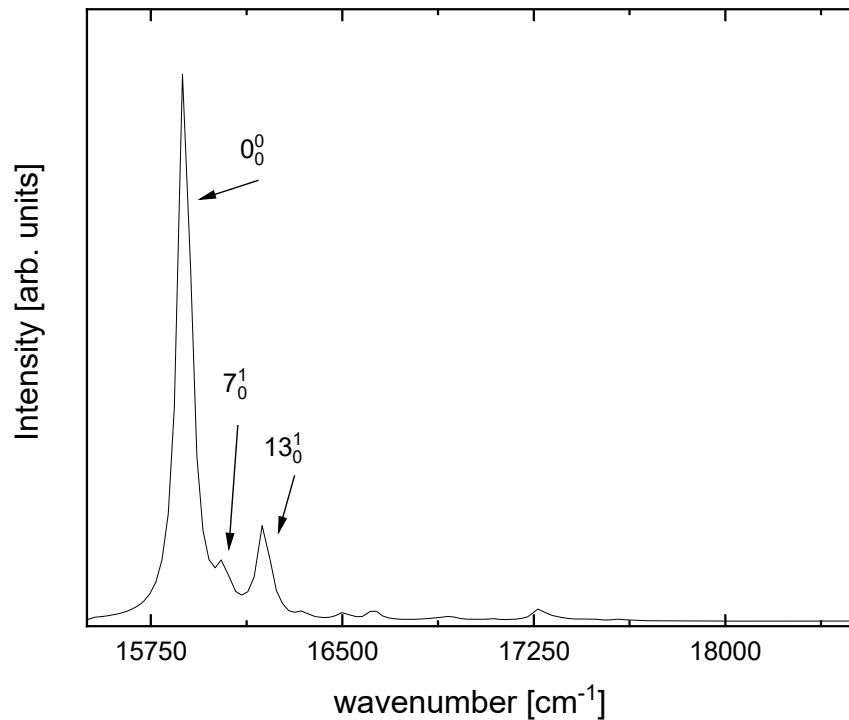
^(a)Supersonic jet experiment, from ref 16.

^(b)This work.

^(c)Numbers in parentheses refer to the placement of point charges in Figure 5.

^(d)Numbers in parentheses describe the shift from mon- to dianion. For scenario 4, the shift is calculated relative to the average of the scenarios 1-3.

S3. Frank-Condon Simulation of Porphine



Franck-Condon simulation of the Q_x band, performed using the $\omega\text{B97XD}/6-31\text{G(d)}$ level of theory (black), with a scaling factor of 0.97 to account for anharmonicity. The 7_0^1 band at 77 cm^{-1} is a macrocycle deformation mode where elongation along the x-axis is out of phase with elongation along the y-axis. The in-phase combination of these motions is the 13_0^1 band and is responsible for the peak at 227 cm^{-1} . See PowerPoint file in Supporting Information for animation of key vibrational modes.

S4. Solvatochromic Data

Table S4. Solvatochromic data for PP (transition energies in cm^{-1})

Solvent / Temperature	pH (charge)	$Q_x(0)^{(a)}$	$Q_x(1)^{(a)}$	$Q_y(0)^{(a)}$	$Q_y(1)^{(a)}$	ref. ^(b)
in vacuo / jet	(0)	15900 ± 100	17420 ± 100	19050 ± 100	20410 ± 100	16
in vacuo / 60	(-1)	15870 ± 10	17400 ± 10	18760 ± 30	20090 ± 20	This work
in vacuo / RT	(-1)	N/A	17210 ± 100	18690 ± 100	20040 ± 100	15
in vacuo / 60	(-2)	15760 ± 10	17280 ± 10	18270 ± 30	19630 ± 30	This work
water / RT	1	15870	16670	18050	19380	14
water / RT	5	15530	16840	17670	18730	14
water / RT	12	15970	17300	18350	19610	14
DMSO / RT	N/A	15870	17330	18450	19760	14

^(a) $Q_x(0)$ and $Q_y(0)$ refer to the maximum of each envelope in the band origin region, while $Q_x(1)$ and $Q_y(1)$ represent the maxima of the envelope in the region of Franck-Condon active modes, ca. 1000 cm^{-1} above each band origin.

^(b) Reference numbers refer to the main text.

S5. Mid-Infrared Spectra of PP

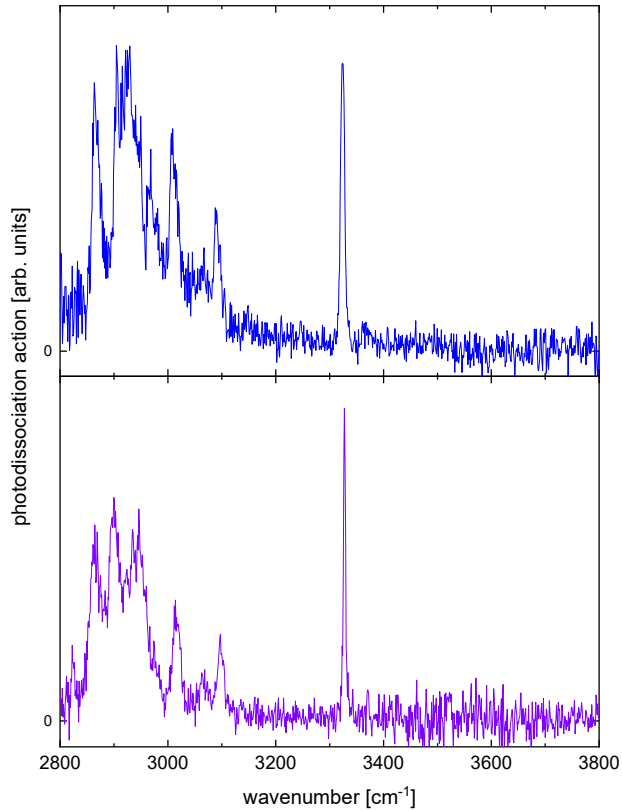


Figure S5. Mid-infrared spectra of $[(\text{PP-H}) \cdot \text{N}_2]^-$ (top panel) and of $[(\text{PP-2H}) \cdot \text{N}_2]^{2-}$ (bottom).

Both spectra show the anti-symmetric NH stretching vibration as intense features at 3324 cm^{-1} and 3327 cm^{-1} , respectively. A subtle feature at 3368 cm^{-1} in the spectrum of the monoanion corresponds to the symmetric stretching mode, which is too weak to be clearly observable in the dianion spectrum. The features below 3200 cm^{-1} are CH stretching vibrations as well as Fermi-resonances of these modes with overtones and combination bands of lower frequency modes. We refrain from explicitly assigning any of these modes due to the high congestion in this region. There is no evidence of a free OH stretching vibration in the spectrum of the monoanion, confirming that the hydrogen is shared between the two carboxylate groups (see Figure 3 in the main text).

S6. Frequencies and Intensities of Vibrational modes of the Q_x Band of Porphine

Transition #	Label	Frequency (1/cm)	Rel. Frequency (1/cm)	Line Intensity	Dipole Strength (a.u.)
1	0> -> 0>	17562.24	0	2442	0.01864
2	0> -> 3 ¹ >	17657.98	95.7363	84.48	0.000684
3	0> -> 7 ¹ >	17715.08	152.8403	415.6	0.003146
4	0> -> 7 ² >	17867.92	305.6807	21.36	0.000161
5	0> -> 13 ¹ >	17873.52	311.2789	561.5	0.004458
6	0> -> 20 ¹ >	17984.46	422.2208	36.3	0.000282
7	0> -> 13 ¹ 7 ¹ >	18026.36	464.1193	87.83	0.000653
8	0> -> 13 ² >	18184.8	622.5579	61.75	0.000477
9	0> -> 33 ¹ >	18295.81	733.5661	511.6	0.003877
10	0> -> 34 ¹ >	18302.44	740.2007	277.9	0.002074
11	0> -> 41 ¹ >	18361.27	799.0247	201	0.001548
12	0> -> 33 ¹ 7 ¹ >	18448.65	886.4064	29.75	0.000226
13	0> -> 34 ¹ 7 ¹ >	18455.29	893.0411	27.27	0.000204
14	0> -> 53 ¹ >	18539.89	977.6411	815	0.005909
15	0> -> 55 ¹ >	18553.53	991.2886	345	0.002639
16	0> -> 58 ¹ >	18585.71	1023.462	286.4	0.002193
17	0> -> 59 ¹ >	18593.21	1030.962	49.16	0.000373
18	0> -> 33 ¹ 13 ¹ >	18607.09	1044.845	79.02	0.000584
19	0> -> 34 ¹ 13 ¹ >	18613.72	1051.48	51.54	0.000376
20	0> -> 61 ¹ >	18624.8	1062.551	498.1	0.003755
21	0> -> 63 ¹ >	18634.17	1071.928	23.43	0.00018
22	0> -> 41 ¹ 13 ¹ >	18672.55	1110.304	32.18	0.000241
23	0> -> 53 ¹ 7 ¹ >	18692.73	1130.481	42.9	0.00031
24	0> -> 55 ¹ 7 ¹ >	18706.37	1144.129	23.3	0.000167
25	0> -> 65 ¹ >	18721.65	1159.405	289.4	0.002198
26	0> -> 58 ¹ 7 ¹ >	18738.55	1176.303	23.85	0.000171
27	0> -> 68 ¹ >	18771.65	1209.407	1103	0.007893
28	0> -> 69 ¹ >	18772.34	1210.099	58.65	0.000421
29	0> -> 61 ¹ 7 ¹ >	18777.64	1215.392	33.17	0.000251
30	0> -> 70 ¹ >	18806.31	1244.064	866.9	0.006291

31	$ 0\rangle \rightarrow 53^113^1\rangle$	18851.16	1288.92	120.4	0.000857
32	$ 0\rangle \rightarrow 55^113^1\rangle$	18864.81	1302.568	55.22	0.000411
33	$ 0\rangle \rightarrow 65^17^1\rangle$	18874.49	1312.245	19.6	0.000139
34	$ 0\rangle \rightarrow 58^113^1\rangle$	18896.99	1334.741	49.6	0.00037
35	$ 0\rangle \rightarrow 68^17^1\rangle$	18924.49	1362.248	74.13	0.000528
36	$ 0\rangle \rightarrow 74^1\rangle$	18930.55	1368.304	1237	0.008754
37	$ 0\rangle \rightarrow 61^113^1\rangle$	18936.07	1373.83	80.68	0.000593
38	$ 0\rangle \rightarrow 75^1\rangle$	18953.21	1390.962	2642	0.01968
39	$ 0\rangle \rightarrow 76^1\rangle$	18953.69	1391.444	1275	0.009568
40	$ 0\rangle \rightarrow 70^17^1\rangle$	18959.15	1396.905	54.83	0.000398
41	$ 0\rangle \rightarrow 78^1\rangle$	18974.28	1412.032	2012	0.01447
42	$ 0\rangle \rightarrow 81^1\rangle$	19011.95	1449.703	86.24	0.00061
43	$ 0\rangle \rightarrow 65^113^1\rangle$	19032.93	1470.683	46.34	0.000343
44	$ 0\rangle \rightarrow 83^1\rangle$	19050.25	1488.006	55.36	0.00039
45	$ 0\rangle \rightarrow 68^113^1\rangle$	19082.93	1520.686	178.4	0.001254
46	$ 0\rangle \rightarrow 74^17^1\rangle$	19083.39	1521.144	78.73	0.000554
47	$ 0\rangle \rightarrow 75^17^1\rangle$	19106.05	1543.803	188.9	0.001415
48	$ 0\rangle \rightarrow 76^17^1\rangle$	19106.53	1544.284	86.25	0.000605
49	$ 0\rangle \rightarrow 70^113^1\rangle$	19117.59	1555.343	138.1	0.00098
50	$ 0\rangle \rightarrow 86^1\rangle$	19119.79	1557.541	76.89	0.000557
51	$ 0\rangle \rightarrow 78^17^1\rangle$	19127.12	1564.873	127.2	0.000915
52	$ 0\rangle \rightarrow 87^1\rangle$	19129.04	1566.798	605.2	0.004457
53	$ 0\rangle \rightarrow 90^1\rangle$	19175.17	1612.931	1720	0.01235
54	$ 0\rangle \rightarrow 91^1\rangle$	19203.18	1640.937	5346	0.03734
55	$ 0\rangle \rightarrow 93^1\rangle$	19241.68	1679.44	2467	0.01824
56	$ 0\rangle \rightarrow 74^113^1\rangle$	19241.83	1679.583	184.1	0.001364
57	$ 0\rangle \rightarrow 75^113^1\rangle$	19264.49	1702.241	440.1	0.003194
58	$ 0\rangle \rightarrow 76^113^1\rangle$	19264.97	1702.723	204.1	0.001491
59	$ 0\rangle \rightarrow 87^17^1\rangle$	19281.88	1719.639	33.86	0.000251
60	$ 0\rangle \rightarrow 78^113^1\rangle$	19285.56	1723.311	320.4	0.002254
61	$ 0\rangle \rightarrow 90^17^1\rangle$	19328.01	1765.771	114.5	0.000824
62	$ 0\rangle \rightarrow 91^17^1\rangle$	19356.02	1793.777	339.9	0.002362
63	$ 0\rangle \rightarrow 93^17^1\rangle$	19394.52	1832.28	168.2	0.001163
64	$ 0\rangle \rightarrow 75^113^17^1\rangle$	19417.33	1855.082	31.53	0.00023
65	$ 0\rangle \rightarrow 78^113^17^1\rangle$	19438.4	1876.152	20.81	0.000146
66	$ 0\rangle \rightarrow 87^113^1\rangle$	19440.32	1878.077	92.67	0.000665

67	$ 0\rangle \rightarrow 90^113^1\rangle$	19486.45	1924.209	277.5	0.001946
68	$ 0\rangle \rightarrow 68^134^1\rangle$	19511.85	1949.608	22.9	0.000163
69	$ 0\rangle \rightarrow 91^113^1\rangle$	19514.46	1952.215	847.1	0.005817
70	$ 0\rangle \rightarrow 93^113^1\rangle$	19552.96	1990.719	393	0.002829
71	$ 0\rangle \rightarrow 75^113^2\rangle$	19575.76	2013.52	34.41	0.000244
72	$ 0\rangle \rightarrow 78^113^2\rangle$	19596.83	2034.59	24.16	0.000167
73	$ 0\rangle \rightarrow 91^113^17^1\rangle$	19667.3	2105.056	55.31	0.000377
74	$ 0\rangle \rightarrow 74^134^1\rangle$	19670.75	2108.505	21.18	0.000148
75	$ 0\rangle \rightarrow 75^134^1\rangle$	19693.41	2131.163	67.57	0.000465
76	$ 0\rangle \rightarrow 76^134^1\rangle$	19693.89	2131.645	23.35	0.000161
77	$ 0\rangle \rightarrow 93^113^17^1\rangle$	19705.8	2143.559	25.45	0.000184
78	$ 0\rangle \rightarrow 78^134^1\rangle$	19714.48	2152.233	35.84	0.000244
79	$ 0\rangle \rightarrow 90^113^2\rangle$	19797.73	2235.488	21.11	0.000145
80	$ 0\rangle \rightarrow 91^113^2\rangle$	19825.74	2263.494	59.84	0.00043
81	$ 0\rangle \rightarrow 93^113^2\rangle$	19864.24	2301.998	29.52	0.000207
82	$ 0\rangle \rightarrow 90^134^1\rangle$	19915.38	2353.131	35.51	0.000239
83	$ 0\rangle \rightarrow 91^134^1\rangle$	19943.38	2381.137	90.94	0.000629
84	$ 0\rangle \rightarrow 75^158^1\rangle$	19976.67	2414.424	29.89	0.00021
85	$ 0\rangle \rightarrow 93^134^1\rangle$	19981.88	2419.641	44.97	0.000306
86	$ 0\rangle \rightarrow 75^168^1\rangle$	20162.61	2600.37	44.38	0.000295
87	$ 0\rangle \rightarrow 91^158^1\rangle$	20226.64	2664.399	26.31	0.000174
88	$ 0\rangle \rightarrow 75^174^1\rangle$	20321.51	2759.266	22.81	0.000159
89	$ 0\rangle \rightarrow 75^2\rangle$	20344.17	2781.924	83.43	0.000571
90	$ 0\rangle \rightarrow 76^175^1\rangle$	20344.65	2782.406	25.31	0.000174
91	$ 0\rangle \rightarrow 78^175^1\rangle$	20365.24	2802.995	39.59	0.000263
92	$ 0\rangle \rightarrow 90^175^1\rangle$	20566.14	3003.893	54.75	0.000363
93	$ 0\rangle \rightarrow 91^175^1\rangle$	20594.14	3031.899	97.6	0.000679
94	$ 0\rangle \rightarrow 93^175^1\rangle$	20632.65	3070.402	48.47	0.000329
95	$ 0\rangle \rightarrow 108^1\rangle$	21184.03	3621.786	20.65	0.000136
96	$ 0\rangle \rightarrow 94^2\rangle$	21498.25	3936.008	125.8	0.000784
97	$ 0\rangle \rightarrow 94^213^1\rangle$	21809.53	4247.287	28.83	0.000188
98	$ 0\rangle \rightarrow 94^233^1\rangle$	22231.8183	4669.5743	26.16	0.0001631
99	$ 0\rangle \rightarrow 94^253^1\rangle$	22475.8933	4913.6493	41.58	0.0002487
100	$ 0\rangle \rightarrow 94^261^1\rangle$	22560.8036	4998.5596	25.39	0.000158
101	$ 0\rangle \rightarrow 94^191^177^1\rangle$	22580.6571	5018.4131	36.32	0.0002169
102	$ 0\rangle \rightarrow 94^191^184^1\rangle$	22670.7491	5108.5051	26.11	0.0001578

103	$ 0\rangle \rightarrow 94^268^1\rangle$	22707.6596	5145.4156	56.16	0.0003322
104	$ 0\rangle \rightarrow 94^270^1\rangle$	22742.3164	5180.0724	44.12	0.0002648
105	$ 0\rangle \rightarrow 94^274^1\rangle$	22866.5559	5304.3119	62.86	0.0003684
106	$ 0\rangle \rightarrow 94^275^1\rangle$	22889.2144	5326.9704	134.3	0.0008285
107	$ 0\rangle \rightarrow 94^276^1\rangle$	22889.6963	5327.4523	64.78	0.0004027
108	$ 0\rangle \rightarrow 94^278^1\rangle$	22910.2847	5348.0407	102.2	0.0006088
109	$ 0\rangle \rightarrow 94^287^1\rangle$	23065.0506	5502.8066	30.71	0.0001876
110	$ 0\rangle \rightarrow 94^290^1\rangle$	23111.1827	5548.9387	87.24	0.0005196
111	$ 0\rangle \rightarrow 94^291^1\rangle$	23139.1887	5576.9447	271.1	0.001571
112	$ 0\rangle \rightarrow 94^293^1\rangle$	23177.6920	5615.4480	125.1	0.0007677
113	$ 0\rangle \rightarrow 94^291^113^1\rangle$	23450.4676	5888.2236	42.84	0.0002448

S7. Frequencies and Intensities of Vibrational modes of the Q_x Band of (PP-H)⁻

Transition #	Label	Frequency (1/cm)	Rel. Frequency (1/cm)	Line Intensity	Dipole Strength (a.u.)
1	$ 0\rangle \rightarrow 0\rangle$	9021.4701	0	169.1	0.002512
2	$ 0\rangle \rightarrow 1^1\rangle$	9041.2763	19.8062	402	0.006054
3	$ 0\rangle \rightarrow 2^1\rangle$	9046.7473	25.2772	162.8	0.002416
4	$ 0\rangle \rightarrow 3^1\rangle$	9055.3662	33.8961	129.4	0.001922
5	$ 0\rangle \rightarrow 8^1\rangle$	9088.1167	66.6466	127.8	0.001899
6	$ 0\rangle \rightarrow 17^1\rangle$	9137.0671	115.597	115.2	0.001713
7	$ 0\rangle \rightarrow 42^1\rangle$	9345.4585	323.9884	101.9	0.001488
8	$ 0\rangle \rightarrow 43^1\rangle$	9359.5519	338.0818	197.9	0.002848
9	$ 0\rangle \rightarrow 46^1\rangle$	9394.9536	373.4835	247.8	0.003653
10	$ 0\rangle \rightarrow 48^1\rangle$	9430.1697	408.6996	135.4	0.001925
11	$ 0\rangle \rightarrow 49^1\rangle$	9449.678	428.2079	93.56	0.001353
12	$ 0\rangle \rightarrow 52^1\rangle$	9513.9112	492.4411	133	0.001915
13	$ 0\rangle \rightarrow 53^1\rangle$	9521.7206	500.2505	107.6	0.001545
14	$ 0\rangle \rightarrow 54^1\rangle$	9532.3791	510.909	92.46	0.001369
15	$ 0\rangle \rightarrow 61^1\rangle$	9640.4841	619.014	400.4	0.005622

16	$ 0\rangle \rightarrow 63^1\rangle$	9667.9472	646.4771	129.8	0.001883
17	$ 0\rangle \rightarrow 65^1\rangle$	9689.2071	667.737	102.9	0.001445
18	$ 0\rangle \rightarrow 67^1\rangle$	9701.334	679.8639	756.6	0.011117
19	$ 0\rangle \rightarrow 74^1\rangle$	9749.2372	727.7671	93.45	0.001371
20	$ 0\rangle \rightarrow 76^1\rangle$	9768.1353	746.6652	136	0.00188
21	$ 0\rangle \rightarrow 78^1\rangle$	9791.1663	769.6962	381.5	0.005239
22	$ 0\rangle \rightarrow 79^1\rangle$	9795.8846	774.4145	155.3	0.002221
23	$ 0\rangle \rightarrow 82^1\rangle$	9814.2044	792.7343	101.7	0.00139
24	$ 0\rangle \rightarrow 87^1\rangle$	9871.6158	850.1457	803.1	0.01096
25	$ 0\rangle \rightarrow 101^1\rangle$	10022.5209	1001.051	209.5	0.002804
26	$ 0\rangle \rightarrow 103^1\rangle$	10035.5796	1014.11	207.5	0.002886
27	$ 0\rangle \rightarrow 118^1\rangle$	10172.9352	1151.465	122	0.001706
28	$ 0\rangle \rightarrow 122^1\rangle$	10198.7353	1177.265	381.2	0.005018
29	$ 0\rangle \rightarrow 123^1\rangle$	10215.8787	1194.409	360.6	0.004761
30	$ 0\rangle \rightarrow 125^1\rangle$	10241.0716	1219.602	165.8	0.002201
31	$ 0\rangle \rightarrow 126^1\rangle$	10245.9435	1224.473	211.5	0.002767
32	$ 0\rangle \rightarrow 128^1\rangle$	10275.6357	1254.166	142.8	0.001941
33	$ 0\rangle \rightarrow 131^1\rangle$	10311.562	1290.092	971	0.01268
34	$ 0\rangle \rightarrow 134^1\rangle$	10334.1165	1312.646	111	0.001441
35	$ 0\rangle \rightarrow 136^1\rangle$	10347.8419	1326.372	369.7	0.005004
36	$ 0\rangle \rightarrow 141^1\rangle$	10395.0622	1373.592	121	0.001614
37	$ 0\rangle \rightarrow 142^1\rangle$	10396.5576	1375.088	238.4	0.003244
38	$ 0\rangle \rightarrow 145^1\rangle$	10413.5682	1392.098	191.5	0.002465
39	$ 0\rangle \rightarrow 146^1\rangle$	10424.885	1403.415	828.5	0.01079
40	$ 0\rangle \rightarrow 149^1\rangle$	10467.9235	1446.453	135.9	0.00182
41	$ 0\rangle \rightarrow 159^1\rangle$	10536.5956	1515.126	142.4	0.00183
42	$ 0\rangle \rightarrow 161^1\rangle$	10546.4583	1524.988	255.9	0.003342
43	$ 0\rangle \rightarrow 170^1\rangle$	10561.4592	1539.989	494.7	0.006387
44	$ 0\rangle \rightarrow 172^1\rangle$	10570.9289	1549.459	103.5	0.001355
45	$ 0\rangle \rightarrow 175^1\rangle$	10589.1221	1567.652	142.9	0.001926
46	$ 0\rangle \rightarrow 176^1\rangle$	10610.6902	1589.22	296.3	0.003855
47	$ 0\rangle \rightarrow 177^1\rangle$	10625.6609	1604.191	126.7	0.001629
48	$ 0\rangle \rightarrow 178^1\rangle$	10638.2643	1616.794	283.6	0.003575
49	$ 0\rangle \rightarrow 179^1\rangle$	10663.5007	1642.031	106.6	0.001345
50	$ 0\rangle \rightarrow 181^1\rangle$	10671.3131	1649.843	399.5	0.005036
51	$ 0\rangle \rightarrow 182^1\rangle$	10685.8685	1664.398	276.7	0.003471

52	$ 0\rangle \rightarrow 183^1\rangle$	10710.7534	1689.283	2575	0.03228
53	$ 0\rangle \rightarrow 184^1\rangle$	10719.9502	1698.48	235.3	0.002962
54	$ 0\rangle \rightarrow 185^1\rangle$	10722.9216	1701.452	263.2	0.003398
55	$ 0\rangle \rightarrow 187^1\rangle$	11147.7066	2126.237	177.4	0.002225

S8. Assignment of FCHT simulation of (PP-H)⁻ under vertical gradient approximation

